Bioartificial Sinus Node Constructed via In Vivo Gene Transfer of an Engineered Pacemaker HCN Channel Reduces the Dependence on Electronic Pacemaker in a Sick-Sinus Syndrome Model

Hung-Fat Tse, Tian Xue, Chu-Pak Lau, Chung-Wah Siu, Kai Wang, Qing-Yong Zhang, Gordon F. Tomaselli, Fadi G. Akar and Ronald A. Li

Circulation 2006;114;1000-1011; originally published online Aug 21, 2006;
DOI: 10.1161/CIRCULATIONAHA.106.615385
Circulation is published by the American Heart Association. 7272 Greenville Avenue, Dallas, TX 72514
 Print ISSN: 0009-7322. Online ISSN: 1524-4539

Bioartificial Sinus Node Constructed via In Vivo Gene Transfer of an Engineered Pacemaker HCN Channel Reduces the Dependence on Electronic Pacemaker in a Sick-Sinus Syndrome Model

Hung-Fat Tse, MD; Tian Xue, PhD; Chu-Pak Lau, MD; Chung-Wah Siu, MBBS; Kai Wang, BS; Qing-Yong Zhang, MD; Gordon F. Tomaselli, MD; Fadi G. Akar, PhD; Ronald A. Li, PhD

Background—The normal cardiac rhythm originates in the sinoatrial (SA) node that anatomically resides in the right atrium. Malfunction of the SA node leads to various forms of arrhythmias that necessitate the implantation of electronic pacemakers. We hypothesized that overexpression of an engineered HCN construct via somatic gene transfer offers a flexible approach for fine-tuning cardiac pacing in vivo.

Methods and Results—Using various electrophysiological and mapping techniques, we examined the effects of in situ focal expression of HCN1-ΔΔΔ, the S3-S4 linker of which has been shortened to favor channel opening, on impulse generation and conduction. Single left ventricular cardiomyocytes isolated from guinea pig hearts preinjected with the recombinant adenovirus Ad-CMV-GFP-IRES-HCN1-ΔΔΔ in vivo uniquely exhibited automaticity with a normal firing rate (237±12 bpm). High-resolution ex vivo optical mapping of Ad-CGI-HCN1-ΔΔΔ–injected Langendorff-perfused hearts revealed the generation of spontaneous action potentials from the transduced region in the left ventricle. To evaluate the efficacy of our approach for reliable atrial pacing, we generated a porcine model of sick-sinus syndrome by guided radiofrequency ablation of the native SA node, followed by implantation of a dual-chamber electronic pacemaker to prevent bradycardia-induced hemodynamic collapse. Interestingly, focal transduction of Ad-CGI-HCN1-ΔΔΔ in the left atrium of animals with sick-sinus syndrome reproducibly induced a stable, catecholamine-responsive in vivo "bioartificial node" that exhibited a physiological heart rate and was capable of reliably pacing the myocardium, substantially reducing electronic pacing.

Conclusions—The results of the present study provide important functional and mechanistic insights into cardiac automaticity and have further refined an HCN gene–based therapy for correcting defects in cardiac impulse generation. **(*Circulation*. 2006;114:1000-1011.)**

Key Words: sinoatrial node ■ pacemakers ■ therapy ■ engineering ■ ion channels

The normal cardiac rhythm originates in the sinoatrial (SA) node that anatomically resides in the right atrium (RA). Malfunctions of the SA node due to aging or disease lead to various forms of arrhythmias that necessitate the implantation of electronic pacemakers. I_f, encoded by the hyperpolarization-activated cyclic-nucleotide–modulated (HCN) channel gene family,[1] is a key player in pacing, although its mechanistic role remains to be fully dissected. Pathophysiologically, human HCN mutations have been linked to sinus node dysfunction.[2,3] To date, 4 isoforms, namely, HCN1, HCN2, HCN3, and HCN4, each with a distinct pattern of tissue distribution and biophysical profiles, have been identified.[4–9] Of the 2 predominant isoforms in the SA node, time-dependent HCN1 currents open ≈40 times faster than those of HCN4 channels[10–14]; the fastest isoform, HCN1, activates at approximately −80 mV, with opening time constants in the range of seconds.

Editorial p 986

HCN1, HCN2, HCN3, and HCN4 readily coassemble (except between HCN2 and HCN3) in different stoichiometries to form heterotetramers with properties that cannot be readily predicted from the individual isoforms.[10,15,16] Therefore, native I_f has a complex molecular identity that depends

Received January 19, 2006; revision received June 20, 2006; accepted June 30, 2006.

From the Department of Medicine, Queen Mary Hospital (H.-F.T., C.-P.L., C.-W.S., K.W., Q.-Y.Z., R.A.L.), University of Hong Kong, Hong Kong; Department of Medicine, Johns Hopkins University (G.F.T., F.G.A.), Baltimore, Md; Department of Cell Biology and Human Anatomy (T.X., C.-W.S., R.A.L.) and Stem Cell Program (T.X., R.A.L.), University of California, Davis, Calif; and Institute of Pediatric Regenerative Medicine, Shriners Hospital for Children of North America (R.A.L.), Sacramento, Calif.

The online-only Data Supplement can be found with this article at http://circ.ahajournals.org/cgi/content/full/CIRCULATIONAHA.106.615385/DC1.

Correspondence to Ronald Li, PhD, Associate Professor, Stem Cell Program, University of California, Room 650, Shriners Hospital, 2425 Stockton Blvd, Sacramento, CA 95817. E-mail ronaldli@ucdavis.edu

Circulation **is available at http://www.circulationaha.org** **DOI: 10.1161/CIRCULATIONAHA.106.615385**

on the species, tissue type, and particular isoforms expressed. Furthermore, HCN channels activate at more positive voltages in neonatal cardiomyocytes (CMs) than in their adult counterparts and other mammalian expression systems, which suggests that the gating properties of I_f are also highly context-dependent.[17] Although overexpression of HCN1 or HCN2 in spontaneously firing, I_f-expressing neonatal left ventricular (LV) cells hastens their firing rate,[18,19] neither of the wild-type (WT) channels alone suffices to induce pacing in quiescent adult LV CMs that intrinsically lack I_f presumably due to their negative activation profiles.[20] Thus, native I_f is difficult to reproduce by simple expression of a single HCN isoform. Here, we took advantage of the engineered construct HCN1-*EVY235-7*ΔΔΔ (or HCN1-ΔΔΔ) channels, the S3-S4 linker of which has been systematically shortened by deleting residues 235 to 237 to favor channel opening[21,22] and thereby compensate for any context-dependent gating effects. We conjectured that overexpressing *EVY235-7*ΔΔΔ channels alone in atrial or ventricular CMs can sufficiently mimic the heteromultimeric native nodal I_f without the need for simultaneous manipulation of the expression levels of multiple HCN isoforms and/or other modifying subunits and factors that may be present in nodal but not muscle cells. Indeed, our experiments show that HCN1-ΔΔΔ channels, when expressed in native ventricular or atrial CMs, exhibit biophysical properties that better mimic those of the heteromultimeric native nodal I_f than WT channels. To further explore the potential of engineered HCN channels for therapies, the effects of in situ focal expression of HCN1-ΔΔΔ in the left atrium (LA) or LV on impulse generation and conduction were examined with various ex vivo and in vivo mapping techniques.

Methods

Adenovirus-Mediated Gene Transfer

Polymerase chain reaction–based mutagenesis of mouse HCN1 (generously provided by Dr Steve Siegelbaum, Columbia University, New York, NY) of the bicistronic adenovirus shuttle vector pAdCMV-GFP-IRES (or pAdCGI) was performed with overlapping oligonucleotides as described in our previous publications.[22,23] The internal ribosomal entry site allows the simultaneous translation of 2 transgenes with a single transcript, and in the present experiments, green fluorescent protein (GFP) and an HCN1 construct. HCN1-ΔΔΔ was cloned into the second position of pAdCGI at *Eco*RI and *Xma*I to generate pAdCGI-HCN1-ΔΔΔ. Adenoviruses were generated by Cre-lox recombination of purified *ψ5* viral DNA and shuttle vector DNA with Cre4 cells. The recombinant products were plaque purified, amplified, and purified again by CsCl gradients, which yielded concentrations of the order of 10^{10} plaque-forming units (PFU) mL^{-1}.

Intracardiac Injection and Isolation of LV CMs

Adenoviruses (150 μL) with a concentration on the order of 10^{10} PFU/mL were injected subepicardially with a 21-gauge needle into the LV anterior wall (≈1 mm deep) of anesthetized adult breeder guinea pigs (weight ≈250 g; Charles River Laboratories, Wilmington, Mass) after thoracotomy and during transient cross-clamping of the great vessels. The area of injection (anterior epicardium, midway between the apex and base) was chosen because it is most suitable for mapping owing to minimal heart curvature; thus, motion artifacts can be suppressed by gentle stabilization. A small suture in the immediate vicinity of the injected area was typically introduced at the time of injection to further assist our identification of the region of interest during the mapping experiments. Furthermore, a parallel optical port was designed to enable visualization of the exact mapped area, which was aligned to include the injected region and its surroundings. Injected animals were allowed to recover from the surgical procedure for 72 to 96 hours. For isolation of CMs, animals were euthanized by intraperitoneal injection of pentobarbital (80 mg/kg). The hearts were quickly excised, followed by perfusion with enzymatic solutions using a customized Langendorff apparatus (Harvard Apparatus, Holliston, Mass) as described previously,[24] and recorded within 24 hours. As needed, porcine atrial CMs were similarly isolated. A typical image of positively transduced LV CMs freshly isolated from an injected heart is provided in Figure I of the online Data Supplement.

High-Resolution Ex Vivo Optical Mapping

To determine whether focal transduction could capture the myocardium, we used the same animal model and optical mapping system that we recently reported.[24] In brief, after surgical dissection of the RA, a specialized cryoprobe was inserted into the right ventricular (RV) cavity and placed in contact with the high septum, 1 mm below the base of the heart; liquid nitrogen was then rapidly and continuously passed through the probe via a commercially available cryogun (Brymill Inc, Ellington, Conn) for 2 minutes, which resulted in ablation of the RV-facing septum and the endocardial surface of the basal RV free wall but not the LV. This procedure resulted in a marked suppression of the intrinsic guinea pig heart rate (<10 bpm). Hearts were then stained with the voltage-sensitive dye di-4-ANEPPS (Invitrogen, Molecular Probes, Eugene, Ore) and placed in a custom-designed, temperature-controlled imaging chamber for optical measurement of action potentials (APs).

Porcine Sick-Sinus Syndrome Model and Catheter-Based Gene Transfer

Anesthesia of miniswine (weight 45 to 55 kg) was performed by intravenous injection of propofol and isoflurane (1%) with intubation and mechanical ventilation. After vascular access was obtained via femoral venous cutdown, a 7F electrophysiological catheter (Biosense Webster, Diamond Bar, Calif) was introduced into the RA and navigated to the SA node located between the junction of superior vena cava and high RA. Radiofrequency energy was then delivered with a Stockert 70 RF generator (Biosense Webster) in the temperature control mode and maximum output set at 50°C and 35 W, respectively, at sites exhibiting the earliest endocardial activation during sinus rhythm. Repeated episodes of radiofrequency ablation up to 60 seconds in duration were delivered until sinus dysfunction occurred, as evidenced by a marked reduction in the baseline sinus rate (to <35 bpm). After ablation, we implanted a dual-chamber pacemaker (Medtronic Inc, Minneapolis, Minn, or Guidant Corp, St Paul, Minn) with 1 lead positioned at the high anterolateral wall of the RA and another at the RV apex to provide supportive pacing if the mean heart rate dropped below 60 bpm. Through a left thoracotomy, AdCGI-HCN1-ΔΔΔ (2×10^{10} PFU) or saline (2 to 3 mL) was injected in the LA appendage. A metal clip was used to mark the injection site. The location was further confirmed by immunohistochemistry. AdCGI-HCN1-ΔΔΔ–injected hearts were fixed in formalin (10%) and embedded in paraffin. Paraffin sections (4 μm) were cut, deparaffinized, rehydrated, and incubated in 10% normal goat serum (Chemicon, Temecula, Calif). Rabbit polyclonal anti-GFP antibody (1:100, Santa Cruz Biotechnology, Inc, Santa Cruz, Calif) was added and incubated at 4°C overnight. After blocking in 3% H_2O_2 in methanol, the positive signals were visualized by the Dako Envision+ kit (Dako, Glostrup, Denmark). Preimmune serum was used as a negative control. Whereas adenoviruses with concentrations ≈10-fold higher than that used in the present study can lead to intense inflammation followed by loss of transgene expression,[25] only a very limited inflammatory response, as qualitatively assessed by visual inspection, was noted in our experiments. In any event, phenotypic changes were not observed between sham and Ad-CGI–injected groups.

Electroanatomic Mapping

Ten to 14 days after the injection procedure, we assessed the endocardial activation patterns in animals with sick-sinus syndrome (SSS) by detailed electroanatomic mapping of the atria. A nonfluoroscopic magnetic electroanatomic system (CARTO; Biosense Webster) was used to measure the spatial distribution of local endocardial activation times relative to a reference electrogram. By moving the mapping catheter to different locations in the RA and LA during spontaneous or atrially paced beats, a color-coded 3-dimensional endocardial activation map was constructed (red, earliest activation; purple, latest activation). Normal sinus rhythm in nonablated animals was also mapped for reference.

Cellular Electrophysiology

Electrical recordings were performed with the whole-cell patch-clamp technique with an Axopatch 200B amplifier and the software pClamp 9.2 (Axon Instruments Inc, Foster City, Calif). A xenon arc lamp was used to view GFP fluorescence at 488/530 nm (excitation/emission). Successfully transduced cells were recognized by their green epifluorescence. Patch pipettes were prepared from 1.5-mm thin-walled borosilicate glass tubes with a Sutter micropipette puller P-97 (Sutter Instrument, Novato, Calf) and had typical resistances of 3 to 5 MΩ when filled with an internal solution containing (in mmol/L): KCl 20; $MgCl_2$ 1; Na-GTP 0.1; Mg-ATP 5; Na_2-phosphocreatine 5; EGTA 1; HEPES 10; pH adjusted to 7.3 with KOH. The external bath solution was composed of (in mmol/L): NaCl 140; KCl 5; glucose 10; $MgCl_2$ 1; $CaCl_2$ 1; HEPES 10; pH adjusted to 7.4 with NaOH. Voltage- and current-clamp recordings were performed at body temperatures (≈37°C). For voltage-clamp recording of I_f, $CdCl_2$ 200 μmol/L and 4-aminopyridine 4 mmol/L were added to block $I_{Ca,L}$, and I_{to}, respectively. For current-clamp recording of APs, the stimulating current was 5 ms in duration. The data presented here have not been corrected for the junction potential (15.1 mV).

Electrophysiological Protocols and Data Analysis

To elicit inward currents, cells were held at −30mV and pulsed from 0 to −140 mV with 10-mV increments for 2 seconds, followed by a 1-second −100-mV pulse. I_f was defined as the 10 μmol/L ZD7288-sensitive, 1-mmol/L Ba^{2+}–insensitive, time-dependent current and I_{K1} as the 1-mmol/L Ba^{2+}–sensitive current. For recording of APs, cells were held at 0 pA without stimulation (for electrically active cells) or with a stimulation of 0.1 to 1 nA/5 ms to elicit a response.

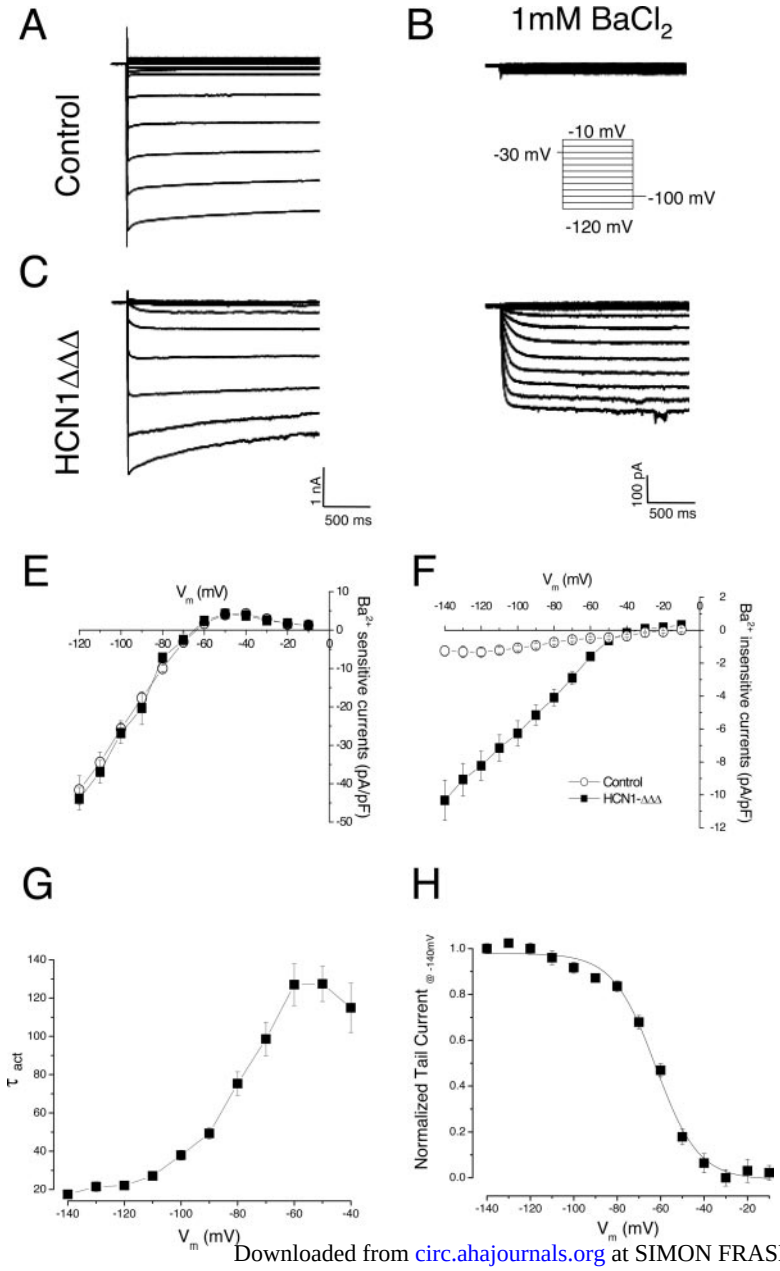

Figure 1. Ba^{2+}-sensitive I_{K1} (A, C) and Ba^{2+}-subtracted I_f (B, D) recorded from LV CMs freshly isolated from control (open symbols) and Ad-CGI-HCN1-ΔΔΔ–injected (solid symbols) adult guinea pigs as indicated, and their corresponding current-voltage (I-V) relationships (E, F). Activation kinetics (G) and steady state activation (H) of Ad-CGI-HCN1-ΔΔΔ–induced currents.

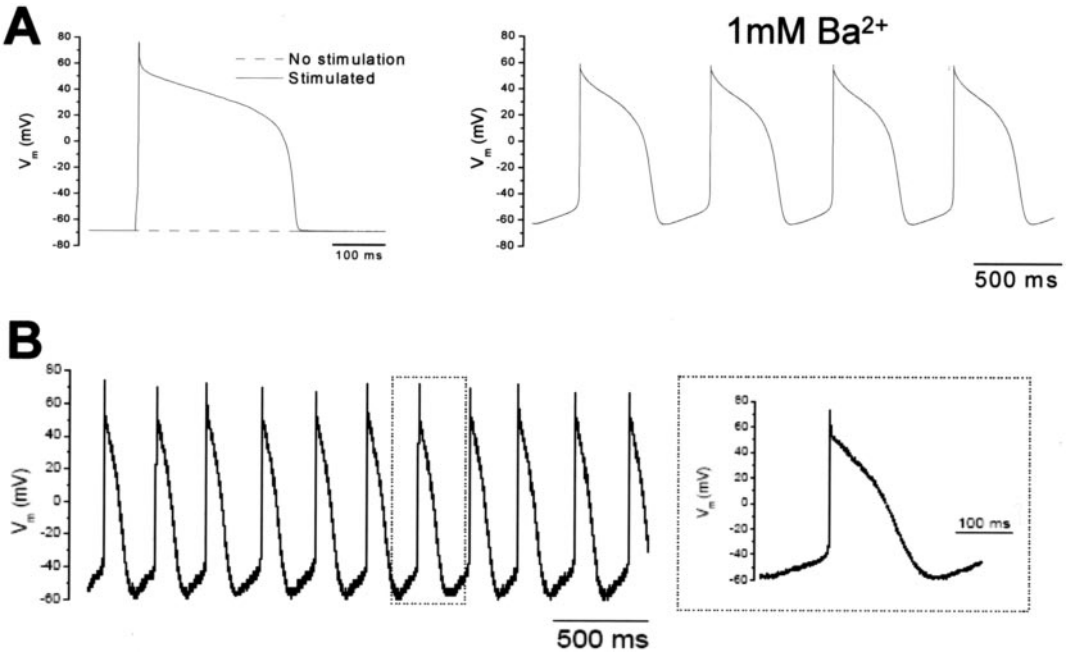

Figure 2. A, Left, AP waveforms of a representative control LV guinea pig cell with (solid line) and without (broken line) stimulation. Right, After the addition of 1-mmol/L Ba^{2+} without stimulation. B, Spontaneously firing APs recorded from a typical LV CM freshly isolated from an Ad-CGI-HCN1-ΔΔΔ–injected animal. The boxed AP is shown in the inset with an expanded time scale.

The voltage dependence of HCN channel activation was assessed by plotting time-dependent tail currents measured immediately after pulsing to −100 mV, normalized to the maximum tail current, as a function of the preceding 2-second test pulse. These recordings were made in the presence of 1-mmol/L $BaCl_2$ to block I_{K1}. Data were fit to the Boltzmann function with the Marquardt-Levenberg algorithm in a nonlinear least-squares procedure:

$$m\infty = \frac{1}{1+e^{[(V_t - V_{1/2})/k]}},$$

where V_t is the test potential, $V_{1/2}$ is the half-point of the relationship, and k=RT/zF is the slope factor. All data reported were mean±SEM, with $P<0.05$ indicating statistical significance as determined with an unpaired Student *t* test.

The authors had full access to the data and take full responsibility for its integrity. All authors have read and agree to the manuscript as written.

Results

Overexpression of HCN1-ΔΔΔ Channels in Guinea Pig LV CMs

Figure 1 shows that I_{K1} (A and E), which could be completely blocked by 1-mmol/L Ba^{2+} (B and F), was robustly expressed in LV CMs freshly isolated from non-Ad-CGI–injected or Ad-CGI–injected adult guinea pig hearts (n=12 from 4 animals). For LV CMs isolated from animals 72 to 96 hours after in vivo gene transfer of Ad-CGI-HCN1-ΔΔΔ via intracardiac injection, a similar Ba^{2+}-sensitive I_{K1} with properties not different from control cells was also expressed (Figure 1C and 1E; $P>0.05$). By contrast, a time-dependent current component, reminiscent of nodal I_f, could be recorded after 1-mmol/L Ba^{2+} subtraction (n=6; Figure 1D). This Ad-CGI-HCN1-ΔΔΔ–induced I_f-like component, sensitive to the known HCN blocker Cs^+ or ZD7288 (data not shown), increased in magnitude and became faster with progressive hyperpolarization (Figure 1F and 1G). The midpoint ($V_{1/2}$) and slope factor (k) derived from the steady-state activation curve were −61.9±1.6 mV and 9.7±1.0, respectively (Figure 1H). Of note, the current density (≈4.5 pA/pF at −80 mV) was comparable to that of native guinea pig pacemaker cells (≈5 pA/pF at −80 mV). Taken together, Ad-CGI-HCN1-ΔΔΔ–induced I_f had properties that largely resembled those of endogenous heteromultimeric nodal I_f.

Ventricular Automaticity Was Observed Exclusively in Ad-CGI-HCN1-ΔΔΔ–Transduced Cardiomyocytes

Shown in Figure 2A (left) is a typical control ventricular cell that was normally electrically quiescent with no spontaneous activity. The resting membrane potential was −76±5 mV (n=7). On injection of a stimulating current (≈0.5 nA for 5 ms), the same cell generated a single AP, which indicates normal excitability. Addition of 1-mmol/L Ba^{2+} to block I_{K1} destabilized the normal resting membrane potential and subsequently resulted in spontaneous firing at an average cycle length of 689±132 ms, which was ≈3-fold slower than that of guinea pig nodal cells (Figure 2A, right), similar to that induced by I_{K1} genetic suppression.[26] Collectively, these observations indicate that although I_{K1} suppression unleashes latent pacemaker activity of ventricular CMs, it is insufficient to reproduce the normal frequency of endogenous nodal pacing.

We next investigated the functional consequences of Ad-CGI-HCN1-ΔΔΔ–mediated I_f overexpression in the AP waveform of LV CMs. Without I_{K1} inhibition, automaticity was exclusively observed in Ad-CGI-HCN1-ΔΔΔ–transduced cells (n=6) but never in control (untransduced or Ad-CGI–transduced) cells. The AP-firing rate (237±12 bpm) was similar to that of the native heart rate of guinea pigs and

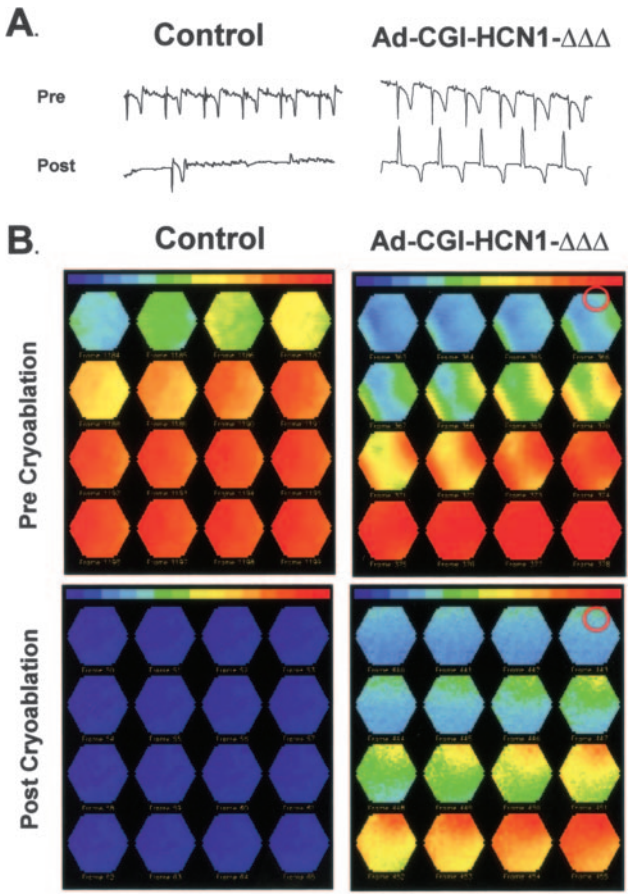

Figure 3. A, Volume-conducted ECGs from representative sham (left) and Ad-CGI-HCN1-ΔΔΔ (right)–preinjected guinea pig hearts in vitro before (Pre) and after (Post) the cryoablation procedure. B, Contour maps of the depolarization wave front recorded every 0.6 ms (from left to right and top to bottom, ie, upper left panels were time zero; blue and red represent hyperpolarization and depolarization, respectively) from a representative guinea pig heart indicating the spread of membrane depolarization (dF/dt) from the injected area (red circle) after the cryoablation procedure in Ad-CGI-HCN1-ΔΔΔ but not control hearts.

much higher than that induced by Ba^{2+} ($P<0.05$) or Kir2.1-AAA.[26] Of note, the maximum diastolic potential (-62 ± 2 mV, n=6; $P<0.05$) was significantly depolarized relative to the resting membrane potential of control LV CMs and was associated with a gradual phase 4 depolarization (slope=0.15 ± 0.02 mV/ms, n=6). These properties were typical of genuine nodal I_f. Nonetheless, the rapid AP upstroke (V=93 ± 15 mV/ms, n=6) and overshoot observed were indicative of the ventricular origin of these rhythmic "pacemaker-like" cells. AP firing of Ad-CGI-HCN1-ΔΔΔ–transduced cells could be silenced by ZD7288 (data not shown).

High-Resolution Ex Vivo Optical Mapping of Ad-CGI-HCN1-ΔΔΔ–Transduced Guinea Pig Hearts

Although we have presented evidence that Ad-CGI-HCN1-ΔΔΔ transduction suffices to confer on single, silent-but-excitable LV CMs automaticity with a normal firing rate, it remains unclear whether focal expression in the intact heart can generate a sufficient depolarizing current source capable of initiating a propagating wave front (due to the electrotonic sink caused by cell-to-cell coupling). Recently, we adopted an ex vivo model of Langendorff-perfused guinea pig hearts in combination with a high-resolution optical AP mapping technique to study the pacemaking ability of electrically active human embryonic stem cell–derived cardiac tissues after in vivo transplantation.[24] Using the same approach, we next attempted to determine whether focal injection of Ad-CGI-HCN1-ΔΔΔ into the LV can produce a functional pacing source.

Shown in Figure 3A are volume-conducted ECGs recorded from representative control and Ad-CGI-HCN1-ΔΔΔ–injected hearts, ex vivo, before and after cryoablation of the AV node. Before ablation, control and Ad-CGI-HCN1-ΔΔΔ–preinjected hearts exhibited similar volume-conducted ECGs (Figure 3A). In fact, the average RR interval (95 ± 14 bpm control, 102 ± 16 bpm Ad-CGI-HCN1-ΔΔΔ, P=NS) and QRS duration (22 ± 4 ms control, 24 ± 6 ms Ad-CGI-HCN1-ΔΔΔ, P=NS) in both groups were comparable. As anticipated, the cryoablation procedure resulted in a marked suppression of the intrinsic rhythm. Interestingly, whereas in control hearts only sporadic, irregular beats (rate <10 bpm) with interrupted episodes of electrical silence were observed

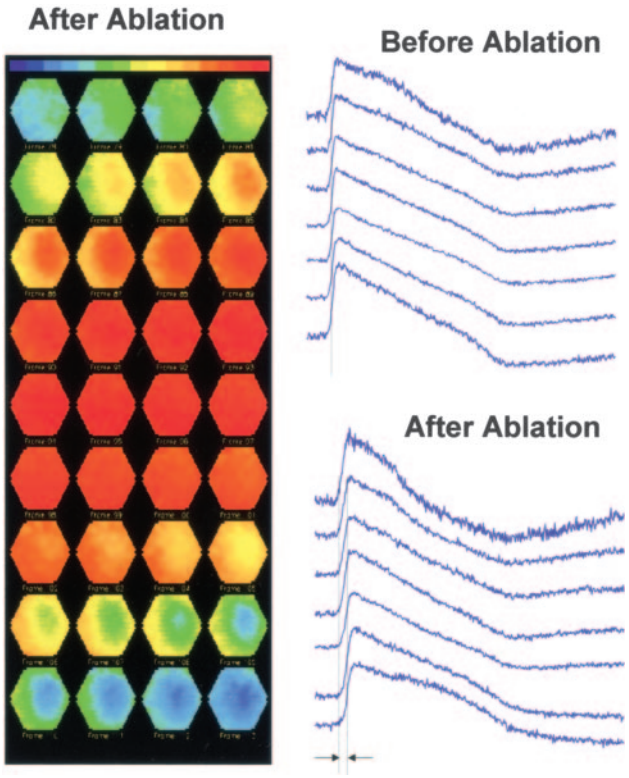

Figure 4. Detailed contour maps of the depolarization wave front (dF/dt) of another Ad-CGI-HCN1-ΔΔΔ–injected heart indicating that the origin of the depolarization wave front arises from the injected area (center). APs are shown from adjacent sites within the mapping field before and after the ablation procedure, indicating sequential time delays between AP upstrokes from the proximal to the distal sites relative to the central injection region in the Ad-CGI-HCN1-ΔΔΔ heart after ablation. Maps were also recorded every 0.6 ms.

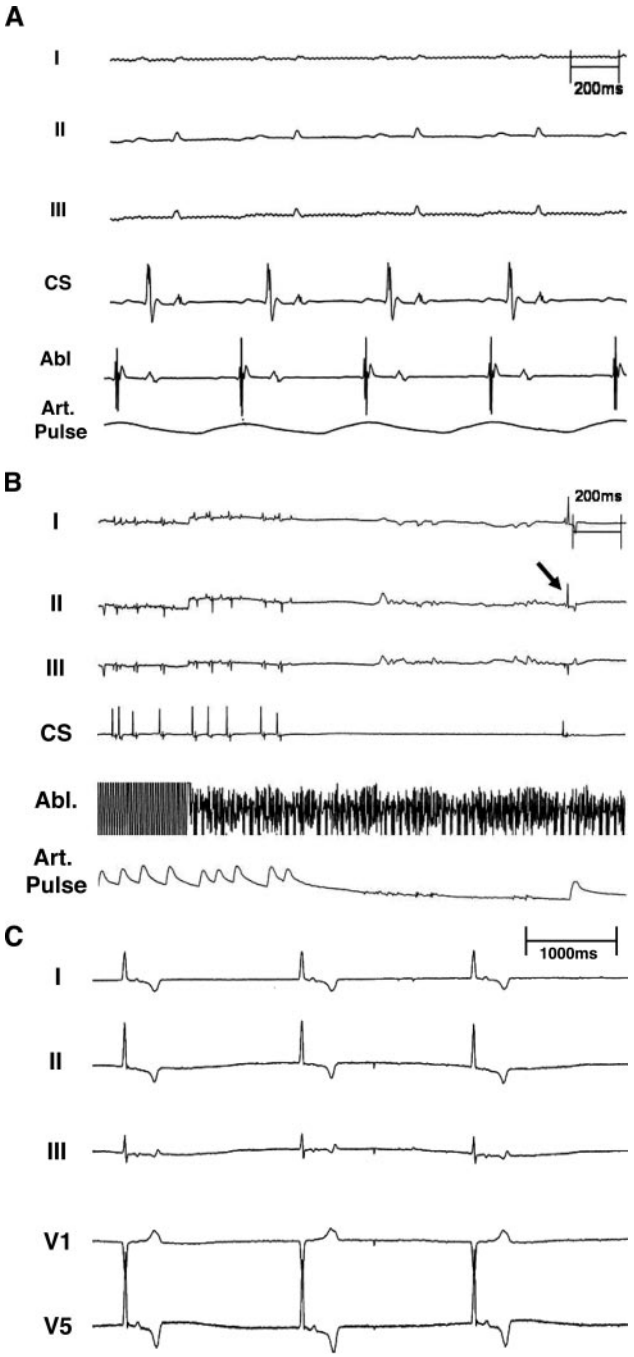

Figure 5. A, Representative tracings on surface ECG (leads I, II, and III), arterial pulse pressure (Art. Pulse), and intracardiac electrograms recorded from coronary sinus (CS) and ablation (Abl) catheter during SA nodal ablation. B, An example of an abrupt response to radiofrequency ablation of the SA node. Shown are leads I, II, and III; an electrogram recorded from CS; and a recording from the ablation catheter in the high lateral RA. Approximately 2 seconds after onset of the tenth application of radiofrequency energy, there was an abrupt termination of sinus rhythm with long periods of asystole before the appearance of a junctional escape rhythm (arrow). C, Surface ECG recording of SSS animals from leads I, II, III, V_1, and V_5 during escape junctional rhythm (rate ≈34 bpm).

(Figure 3A), Ad-CGI-HCN1-ΔΔΔ–injected hearts after cryoablation exhibited a stable, regular rhythm characterized by an inverted T wave and a prolonged (by 68%) QRS duration on the volume-conducted ECG, consistent with an activation spread from a source of ventricular origin (ie, similar to ventricular paced rhythms).

To precisely define the origin of the depolarization wave front in control and Ad-CGI-HCN1-ΔΔΔ–injected hearts, we performed high-resolution optical AP mapping. Shown in Figure 3B are detailed contour maps recorded every 0.6 ms from the epicardial surface of a representative control guinea pig heart that depict the sequential spread of the depolarizing wave front before and after cryoablation of the AV node. In accordance with our previous results, the spread of membrane depolarization of control hearts was very rapid across the epicardial surface (Figure 3B) before cryoablation. Multiple points of epicardial breakthrough from deeper intramyocardial layers were observed, which reflects a normal ventricular activation sequence via the His-Purkinje conduction system (n=9). After cryoablation, however, the same control hearts exhibited a marked loss of rhythmic activity characterized by long episodes of electrical silence (up to several seconds in duration; Figure 3B). This was not due to loss of intrinsic ventricular excitability, because these preparations could be readily paced via unipolar extracellular wires placed on the LV epicardium and LV endocardium (without change in diastolic pacing threshold or epicardial AP duration and morphology[24]).

Interestingly, as in controls, hearts that were preinjected with Ad-CGI-HCN1-ΔΔΔ also exhibited an epicardial wave

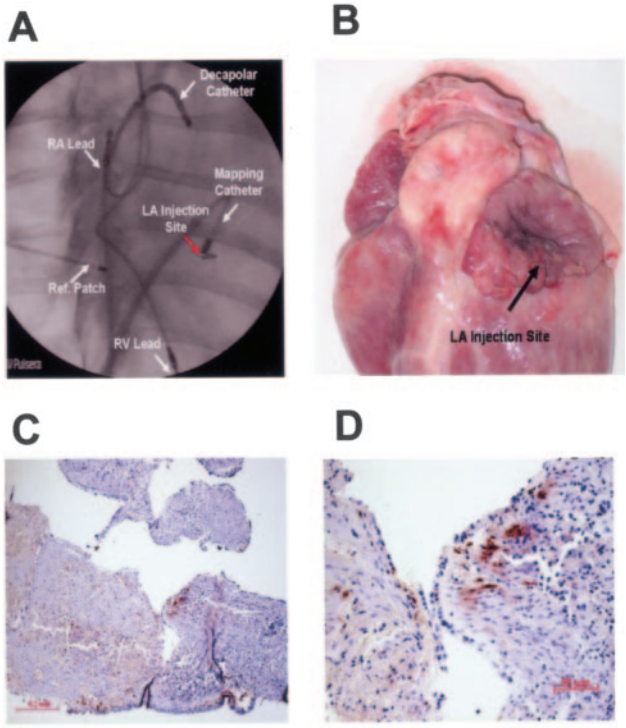

Figure 6. A, Fluoroscopic image showing pacing leads at the RA and the RV apex, the decapolar catheter at the roof of RA against the intra-atrial septum, and the mapping catheter in the LA during electroanatomic mapping. The site of injection was marked by a surgical clip (red arrow). Ref. Patch indicates reference patch for anatomical mapping. B, Gross pathology showing the injection site at the LA appendage (arrow). C and D, Sectioned heart demonstrating the expression of GFP with GFP staining (brown) at low (left) and high (right) magnifications.

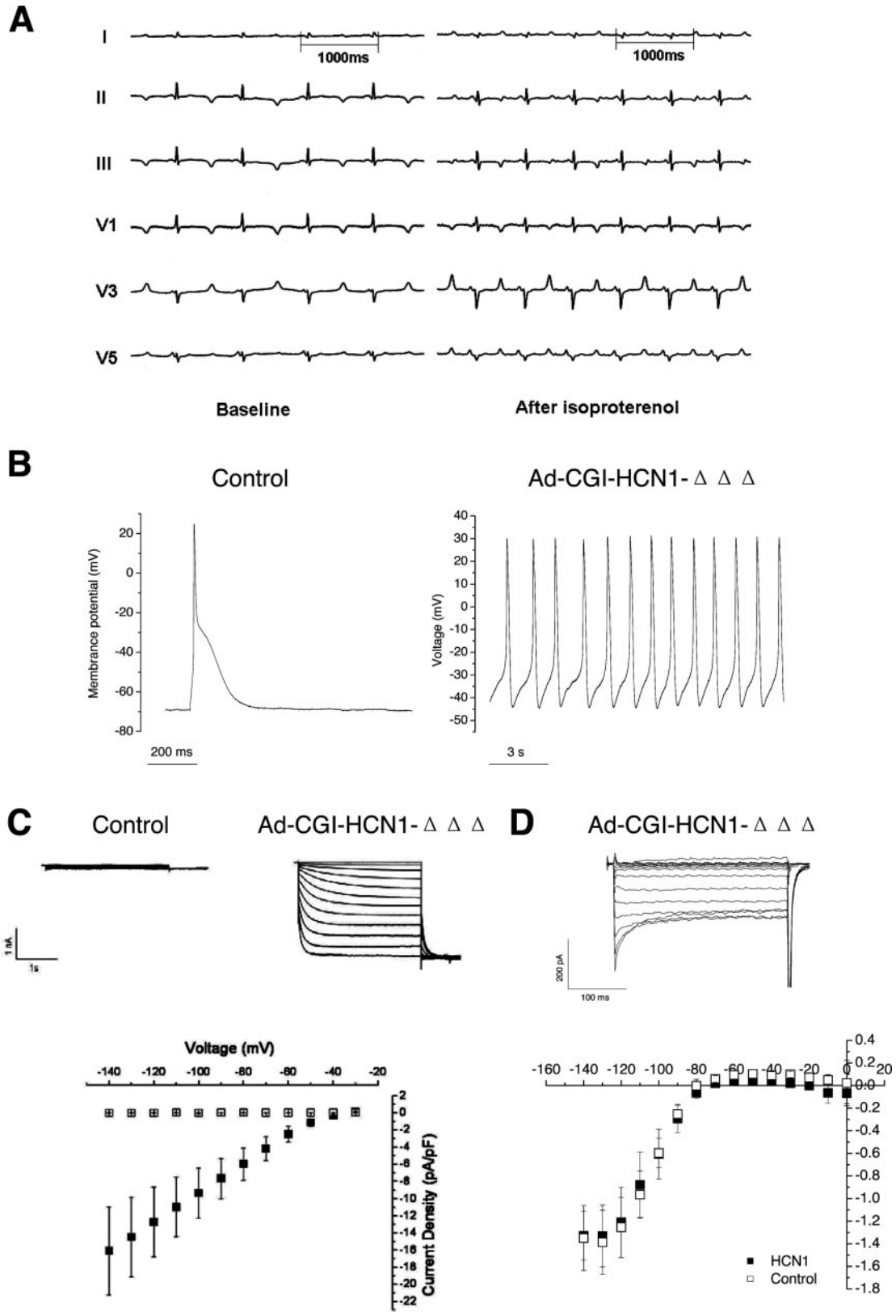

Figure 7. A, Representative surface ECG recording from leads I, II, III, V_1, and V_5 and intracardiac recording from RA and coronary sinus (CS) during baseline sinus rhythm (top) and spontaneous LA rhythm after Ad-CGI-HCN1-ΔΔΔ injection (bottom). Note the differences in P-wave morphology on surface ECG and the activation sequences in the RA and CS electrograms. B, The baseline heart rate of spontaneous LA rhythm of this particular animal was 70 bpm (left), which increased to 98 bpm after 1 $\mu g \cdot min^{-1} \cdot kg^{-1}$ isoproterenol infusion (right). No changes in P-wave morphologies after isoproterenol infusion were noted, which suggests the same origin of the LA rhythm. Typical tracings of (C) AP and (D) I_f recorded from control (left) and Ad-CGI-HCN1-ΔΔΔ–transduced (right) LA cells as indicated, and the corresponding I-V relationships (bottom), are shown. E, I-V relationships of I_{K1} recorded from control and transduced cells.

front breakthrough pattern before cryoablation (Figure 3B, left), which indicates that the effect of focal Ad-CGI-HCN1-ΔΔΔ expression, if any, was masked by the intrinsic junctional rhythm. However, in stark contrast to control preparations, cryoablation in Ad-CGI-HCN1–ΔΔΔ–injected hearts was uniquely associated with an activation wave front that originated from a discrete focal source that corresponded to the injection site and that spread in a planar fashion along the epicardial surface, consistent with a relatively superficial origin (Figure 3B, right). This activation pattern was similar to that induced by electrically active human embryonic stem cell–derived cardiac cells except that the induced rate was markedly higher (Figure 3A). Shown in Figure 4 are contour maps of the depolarizing wave front (left) and APs (right) from adjacent recording sites in another Ad-CGI-HCN1-ΔΔΔ–injected heart. Again, after ablation, a depolarization wave front formed from a discrete source within the mapping field that spread epicardially with a significant time delay (11 ms) compared with before (<2 ms) the procedure (Figure 4, right).

Generating a Porcine SSS Model

Encouraged by our optical mapping experiments, which demonstrated clear successful pacing of the intact LV by preinjection of Ad-CGI-HCN1-ΔΔΔ, we next switched to a large-animal (porcine) model that exhibits an intrinsic baseline sinus rate (78±14 bpm; n=11) and key atrial and ventricular anatomic features more similar to those of humans. We first developed a porcine SSS model by radiofrequency ablation of the SA node to produce sinus node dysfunction and bradycardia (Figure 5A through 5C). To prevent asystole or bradycardia-related hemodynamic compromise after ablation, we implanted a dual-chamber electronic pacemaker with 1 electrode positioned at the high anterolateral wall of the RA and another at the RV apex.

To further validate our porcine SSS model, we closely monitored the heart rhythm of ablated pigs for 2 weeks using pacemaker telemetry monitoring. Indeed, persistent SA node dysfunction was observed in 11 of 14 animals; the electronic pacemaker–recorded heart rate histogram in SSS animals showed that the intrinsic rates were predominantly slower than the lowest programmed rate of 60 bpm and required device-supported atrial electrical stimulations during 78±12% of the monitored period.

Engineering an In Vivo Bioartificial SA Node to Correct SSS via Focal Atrial Transduction of HCN1-ΔΔΔ

We next injected either Ad-CGI-HCN1-ΔΔΔ (n=5), Ad-CGI (n=2), or saline (n=2) into the LA appendage of SSS animals (Figure 6A and 6B). At 10 to 14 days after injection, a stable spontaneous atrial rhythm with an average rate of 64±9 bpm could be detected in Ad-CGI-HCN1-ΔΔΔ–injected SSS animals (Figure 7A). The elevation in intrinsic heart rate reduced the dependence on device-supported atrial pacing from 69±18% to only 14±15% (n=5, $P=0.02$; see Data Supplement Figure II). At baseline in sinus rhythm, intravenous administration of isoproterenol (1 to 2 $\mu g \cdot min^{-1} \cdot kg^{-1}$) increased the sinus rate from 78±12 to 120±9 bpm (n=4, $P<0.01$). Interestingly, the spontaneous atrial rhythm also increased but to a lesser degree (92±10 bpm, n=3) on the administration of isoproterenol (Figure 7B; $P<0.05$) but not atropine (1.8 mg; data not shown; $P>0.05$), which suggests that the reverted normal rhythm was not mediated by vagal input. Indeed, patch-clamp experiments confirmed I_f overexpression and the presence of spontaneous nodal-like APs uniquely in Ad-CGI-HCN1-ΔΔΔ–transduced LA cells (54.6±10.3 bpm and 16±4 pA/pF at −140 mV; Figure 7C and 7D), as anticipated from our guinea pig experiments. By contrast, control LA cells were silent but excitable and had no I_f (0±0 bpm and 0±0 pA/pF; $P<0.01$). Control and transduced LA CMs had identical I_{K1} (−0.85±0.25 pA/pF at −150 mV; $P<0.05$; Figure 7D). The reduced I_{K1} in LA myocytes compared with LV myocytes allows for more manifest effect of virally transduced I_f on diastolic depolarization. When monitored over the same period, neither stable spontaneous atrial rhythm nor I_f was observed in control SSS animals (n=6: 2 uninjected, 2 Ad-CGI–injected, and 2 saline-injected), which indicates that the results observed were not induced by the injection procedure per se.

To confirm the precise pacing origin, we investigated the atrial activation pattern of Ad-CGI-HCN1-ΔΔΔ–transduced SSS animals using electroanatomic mapping.[27] For control (nonablated or sham SSS animals injected with Ad-CGI or saline), endocardial electrical activation was initiated either from the native SA node or the implanted lead, respectively, as anticipated (Figure 8A and 8B). By contrast, activation of Ad-CGI-HCN1-ΔΔΔ–injected porcine hearts originated from the injection site in the LA appendage, with the RA activating last (Figure 8C). The average atrial endocardial activation time was 101±21 ms. Interestingly, this "reversed" activation pattern reverted to those of controls when mapping was performed with device-driven RA pacing at 10 to 15 bpm faster than the spontaneous Ad-CGI-HCN1-ΔΔΔ–induced LA rhythm (Figure 8D): The earliest electrical activation was once again at the high anterolateral RA, which then propagated to the LA with an activation time of 110±32 ms. Immunohistochemical experiments confirmed the localized expression of GFP at the focal injection site (Figure 6B through 6D).

Discussion

Malfunction or loss of sinus node pacemaker cells due to disease or aging often necessitates the implantation of electronic pacemakers. Although effective, the use of such devices may be associated with significant health risks (eg, infection or death), expenditure, and the need for periodic battery and lead replacements. Furthermore, their implementation is particularly difficult for young patients whose hearts are small and growing. The native SA node, the function of which is the sum of a repertoire of numerous ionic mechanisms involving the absence of I_{K1}[28] and the presence of I_{Kr}, ryanodine receptor, and Na^+-Ca^{2+} exchanger,[29] for example, is a complex structure that consists of a gradient of a few thousand nodal cells with a range of phenotypic properties and anatomic boundary effects.[30] In the present study, we demonstrate that overexpressing a single bioengineered HCN construct of relatively few CMs is sufficient to regenerate a

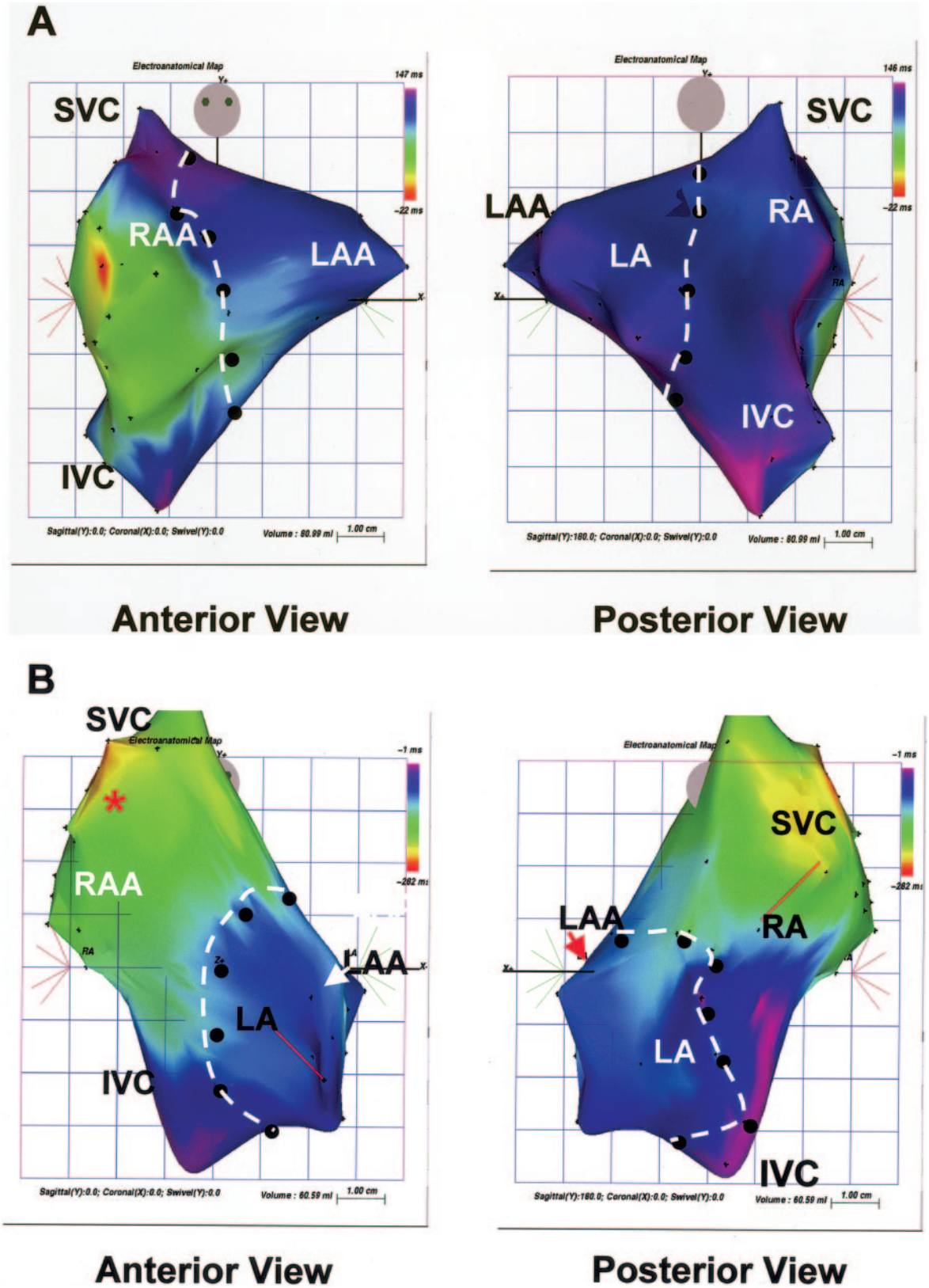

Figure 8. Anterior (left) and posterior (right) view of 3D electroanatomic maps of (A) control (nonablated) animal, (B) SSS animal during RA pacing, and (C) SSS animal after Ad-CGI-HCN1-ΔΔΔ injection demonstrate the atrial endocardial activation patterns in each condition. The borders of the intra-atrial septum were tagged with black spots and connected with white dotted lines to delineate the RA and LA. During sinus rhythm in the control animal, the earliest endocardial activation, initiated in the junction between the superior vena cava (SVC) and RA (red), propagated to the LA (blue-purple). In the SSS animal during RA pacing, the earliest endocardial activation was initiated in the high anterolateral RA (red, asterisk in B) adjacent to the SVC. It then propagated to the LA appendage (LAA) and IVC (blue-purple). For

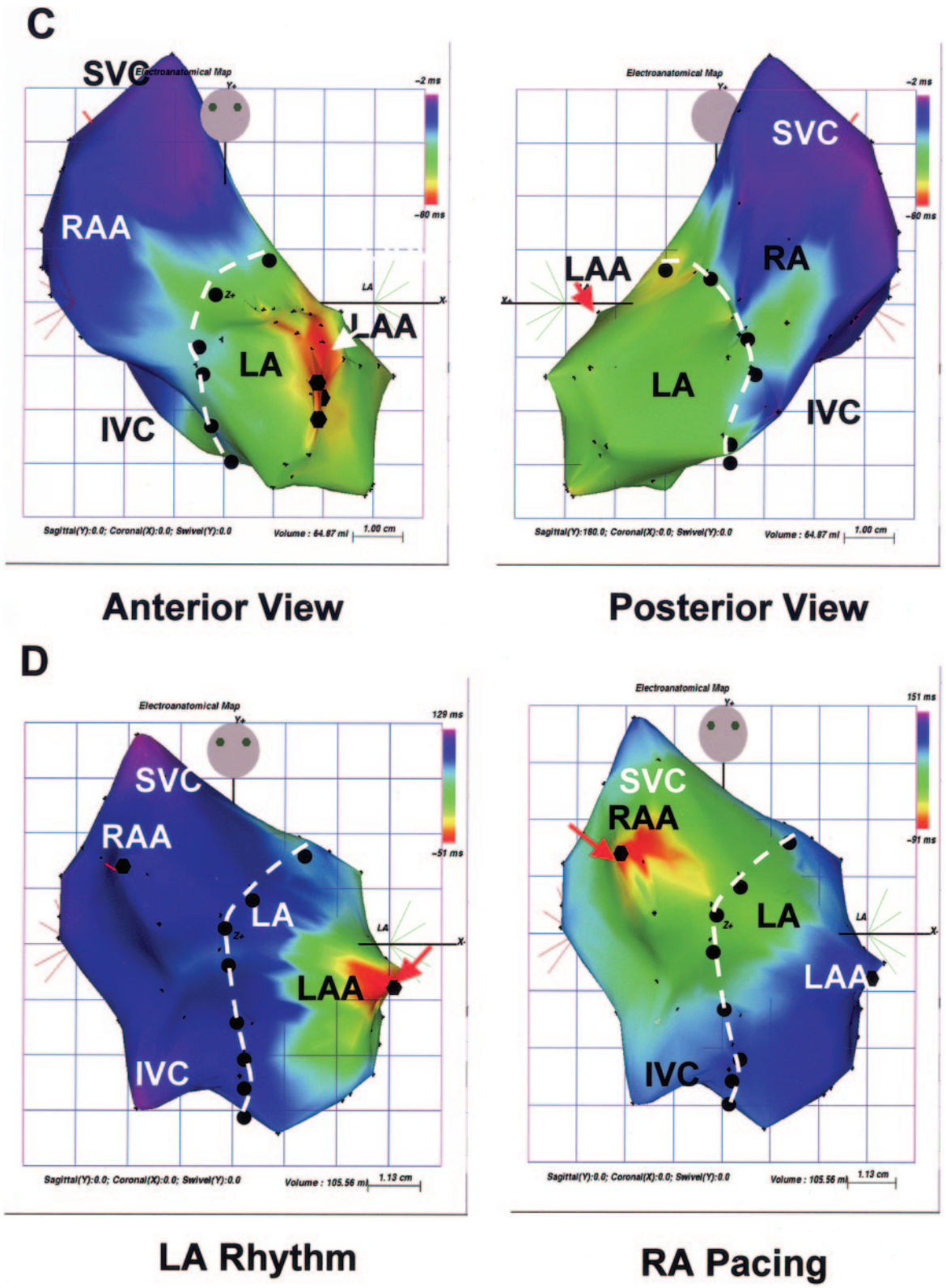

Figure 8. Continued.
spontaneous LA rhythms observed after Ad-CGI-HCN1-ΔΔΔ gene transfer, earliest endocardial activation was initiated at the Ad-CGI-HCN1-ΔΔΔ injection sites (white arrows) and propagated to the RA appendage (RAA), SVC, and IVC (blue-purple). D, Anterior view of 3D electroanatomic maps of SSS animal after Ad-CGI-HCN1-ΔΔΔ injection during spontaneous LA rhythm (left) and RA pacing (right). During RA overdrive pacing, the earliest endocardial activation shifted from the LAA (red, left) to the pacing site in the RA appendage (red, right).

functional bio-SA node in the atrium that stably fires at a physiological rate capable of substituting or supplementing electronic devices in a large SSS animal model with anatomic and physiological features highly relevant to humans. Furthermore, our observation that Ad-CGI-HCN1-ΔΔΔ–induced rhythms can be overridden suggests that gene-based biological pacemakers, like electronic pacemakers, can be "programmed" to activate only after the heart rate has fallen below a preset level by fine-tuning the gating properties of I_f. That said, HCN1-ΔΔΔ is unlikely to be the future choice of therapy given that HCN1 is least sensitive to cAMP and thus neurohormonal regulation. Nonetheless, the present data demonstrate that engineered HCN channels are better candidates for future potential gene-based therapies of SSS, extending previous findings with WT channels.

In addition to HCN overexpression, at least 2 other approaches have been attempted to induce ectopic pacing activity. These include overexpression of β_2-adrenergic receptors in the atria[31] and genetic suppression of ventricular I_{K1}.[26,32] Somatic gene transfer of the dominant-negative construct Kir2.1-AAA in adult guinea pig ventricular myocytes suppressed I_{K1} expression (by ≈80%), leading to the conversion of quiescent ventricular myocytes into "nodal-like" cells in a manner analogous to the Ad-HCN1-ΔΔΔ–transduced cells described here. However, Kir2.1AAA-induced ventricular automaticity, similar to that caused by Ba^{2+} blockade of I_{K1}, was much slower than the normal heart rate, and as such was suboptimal for acting as a reliable biological pacemaker. In other words, I_{K1} acts in a binary fashion to facilitate automaticity without providing a direct means to modulate the induced firing rate required for everyday activities. The present results demonstrate that regulatable ectopic cardiac pacing can be better achieved by modulating a genuine pacemaker current (I_f) rather than by suppressing an inhibitor of spontaneous membrane depolarization.

Although overexpression of WT HCN2 alone did not induce automaticity in isolated cells,[18] it was capable of inducing a slow rhythm when overexpressed in the left bundle branch of animals exposed to vagally mediated sinus arrest.[33,34] It is plausible that the $V_{1/2}$ of the HCN2-induced I_f (−96 versus −61.9 mV in our case) was below the threshold required to cause active pacing in single LV cells.[20] As such, the hurdle of achieving an expressed current that resembles native I_f, the interacting accessory subunits and other modulatory factors of which remain to be fully identified, was overcome in the present study by protein engineering.

Although the present study has direct clinical implications, adenoviral vectors are unlikely to be used as the delivery vehicle. This is because although their transduction efficiency is typically high, adenovirus-mediated transgene expression is transient. Previous in vivo adenoviral gene transfer studies have reported an expression profile that peaks at ≈1 week, plateaus, then declines for a period of ≈3 to 5 weeks. By week 10, no transgene expression could be detected. Our in vivo swine experiments were designed to study the resultant functional consequences during the plateau phase (ie, 1 to 2 weeks after injection) so as to better reflect the outcome achieved by persistent genetic modification. Long-term effects (eg, electrical remodeling) of our approach can be studied with adeno-associated virus, the transgene of which is incorporated into the recipient genome for permanent modification, although a disadvantage is that transgene integration is random and may lead to deleterious consequences. Alternatively, ex vivo genetic modification, as previously demonstrated in human mesenchymal stem cells[35] and human embryonic stem cell–derived CMs,[24,36] followed by detailed genetic analysis before cell transplantation is another attractive option.

Collectively, the present study provides a pragmatic basic and translational platform for constructing gene- or cell-based (eg, embryonic stem cell–derived) pacemakers[24,36] with a range of customized basal oscillation frequency and/or drug sensitivity using engineered ion channels. Such a biological approach is advantageous over electronic devices by maintaining the in vivo responsiveness of pacing to endogenous neuronal and hormonal inputs. We conclude that engineered HCN channels offer a flexible approach to induce and fine-tune pacing. The present results provide important functional and mechanistic insights into cardiac automaticity and have brought closer a potential gene-based therapy for correcting defects in cardiac impulse generation.

Sources of Funding

This work was supported by grants from the National Institutes of Health (R01 HL72857 to Dr Li and HL77180 to Drs Tomaselli and Akar), the Stem Cell Program of the University of California (to Dr Li), the Hong Kong Research Grant Council (HKU 7459/04M to Drs Lau, Tse, and Li), and the Sun Chieh Yeh Heart Foundation Fund (Drs Lau and Tse and C.-W. Siu). Chung-Wah Siu was supported by a postdoctoral fellowship award from the Croucher Foundation.

Disclosures

None.

References

1. Robinson RB, Siegelbaum SA. Hyperpolarization-activated cation currents: from molecules to physiological functions. *Annu Rev Physiol*. 2003;65:453–480.
2. Schulze-Bahr E, Neu A, Friederich P, Kaupp UB, Breithardt G, Pongs O, Isbrandt D. Pacemaker channel dysfunction in a patient with sinus node disease. *J Clin Invest*. 2003;111:1537–1545.
3. Milanesi R, Baruscotti M, Gnecchi-Ruscone T, DiFrancesco D. Familial sinus bradycardia associated with a mutation in the cardiac pacemaker channel. *N Engl J Med*. 2006;354:151–157.
4. Ludwig A, Zong X, Jeglitsch M, Hofmann F, Biel M. A family of hyperpolarization-activated mammalian cation channels. *Nature*. 1998; 393:587–591.
5. Santoro B, Liu DT, Yao H, Bartsch D, Kandel ER, Siegelbaum SA, Tibbs GR. Identification of a gene encoding a hyperpolarization-activated pacemaker channel of brain. *Cell*. 1998;93:717–729.
6. Santoro B, Tibbs GR. The HCN gene family: molecular basis of the hyperpolarization-activated pacemaker channels. *Ann N Y Acad Sci*. 1999;868:741–764.
7. Santoro B, Chen S, Luthi A, Pavlidis P, Shumyatsky GP, Tibbs GR, Siegelbaum SA. Molecular and functional heterogeneity of hyperpolarization-activated pacemaker channels in the mouse CNS. *J Neurosci*. 2000;20:5264–5275.
8. Shi W, Wymore R, Yu H, Wu J, Wymore RT, Pan Z, Robinson RB, Dixon JE, McKinnon D, Cohen IS. Distribution and prevalence of hyperpolarization-activated cation channel (HCN) mRNA expression in cardiac tissues. *Circ Res*. 1999;85:e1–e6.
9. Ludwig A, Zong X, Hofmann F, Biel M. Structure and function of cardiac pacemaker channels. *Cell Physiol Biochem*. 1999;9:179–186.
10. Altomare C, Terragni B, Brioschi C, Milanesi R, Pagliuca C, Viscomi C, Moroni A, Baruscotti M, DiFrancesco D. Heteromeric HCN1-HCN4

channels: a comparison with native pacemaker channels from the rabbit sinoatrial node. *J Physiol*. 2003;549:347–359.
11. Ishii TM, Takano M, Ohmori H. Determinants of activation kinetics in mammalian hyperpolarization-activated cation channels. *J Physiol (Lond)*. 2001;537:93–100.
12. Stieber J, Thomer A, Much B, Schneider A, Biel M, Hofmann F. Molecular basis for the different activation kinetics of the pacemaker channels HCN2 and HCN4. *J Biol Chem*. 2003;278:33672–33680.
13. Seifert R, Scholten A, Gauss R, Mincheva A, Lichter P, Kaupp UB. Molecular characterization of a slowly gating human hyperpolarization-activated channel predominantly expressed in thalamus, heart, and testis. *Proc Natl Acad Sci U S A*. 1999;96:9391–9396.
14. Ludwig A, Zong X, Stieber J, Hullin R, Hofmann F, Biel M. Two pacemaker channels from human heart with profoundly different activation kinetics. *EMBO J*. 1999;18:2323–2329.
15. Chen S, Wang J, Siegelbaum SA. Properties of hyperpolarization-activated pacemaker current defined by coassembly of HCN1 and HCN2 subunits and basal modulation by cyclic nucleotide. *J Gen Physiol*. 2001;117:491–504.
16. Xue T, Marban E, Li RA. Dominant-negative suppression of HCN1- and HCN2-encoded pacemaker currents by an engineered HCN1 construct: insights into structure-function relationships and multimerization. *Circ Res*. 2002;90:1267–1273.
17. Qu J, Altomare C, Bucchi A, DiFrancesco D, Robinson RB. Functional comparison of HCN isoforms expressed in ventricular and HEK 293 cells. *Pflugers Arch*. 2002;444:597–601.
18. Qu J, Barbuti A, Protas L, Santoro B, Cohen IS, Robinson RB. HCN2 overexpression in newborn and adult ventricular myocytes: distinct effects on gating and excitability. *Circ Res*. 2001;89:E8–E14.
19. Er F, Larbig R, Ludwig A, Biel M, Hofmann F, Beuckelmann DJ, Hoppe UC. Dominant-negative suppression of HCN channels markedly reduces the native pacemaker current I_f and undermines spontaneous beating of neonatal cardiomyocytes. *Circulation.* 2003;107:485–489.
20. Azene E, Xue T, Marban E, Tomaselli GF, Li RA. Hysteretic current-voltage behavior of HCN-encoded pacemaker channels: insights into the physiological role of I_f in cardiac pacing. *Cardiovasc Res*. 2006;67:263–273.
21. Tsang SY, Lesso H, Li RA. Critical intra-linker interactions of HCN1-encoded pacemaker channels revealed by interchange of S3-S4 determinants. *Biochem Biophys Res Commun*. 2004;322:652–658.
22. Tsang S, Lesso H, Li RA. Dissecting the structural and functional roles of the S3-S4 linker of pacemaker (HCN) channels by systematic length alterations. *J Biol Chem*. 2004;279:43752–43759.
23. Lesso H, Li RA. Helical secondary structure of the external S3-S4 linker of pacemaker (HCN) channels revealed by site-dependent perturbations of activation phenotype. *J Biol Chem*. 2003;278:22290–22297.
24. Xue T, Cho HC, Akar FG, Tsang SY, Jones SP, Marban E, Tomaselli GF, Li RA. Functional integration of electrically active cardiac derivatives from genetically engineered human embryonic stem cells with quiescent recipient ventricular cardiomyocytes: insights into the development of cell-based pacemakers. *Circulation*. 2005;111:11–20.
25. Quinones MJ, Leor J, Kloner RA, Ito M, Patterson M, Witke WF, Kedes L. Avoidance of immune response prolongs expression of genes delivered to the adult rat myocardium by replication-defective adenovirus. *Circulation*. 1996;94:1394–1401.
26. Miake J, Marban E, Nuss HB. Gene therapy: biological pacemaker created by gene transfer. *Nature*. 2002;419:132–133.
27. Ben-Haim SA, Osadchy D, Schuster I, Gepstein L, Hayam G, Josephson ME. Nonfluoroscopic, in vivo navigation and mapping technology. *Nat Med*. 1996;2:1393–1395.
28. Silva J, Rudy Y. Mechanism of pacemaking in I_{K1}-downregulated myocytes. *Circ Res*. 2003;92:261–263.
29. Lakatta EG, Maltsev VA, Bogdanov KY, Stern MD, Vinogradova TM. Cyclic variation of intracellular calcium: a critical factor for cardiac pacemaker cell dominance. *Circ Res.* 2003;92:45e-50e.
30. Boyett MR, Honjo H, Kodama I. The sinoatrial node, a heterogeneous pacemaker structure. *Cardiovasc Res*. 2000;47:658–687.
31. Edelberg JM, Huang DT, Josephson ME, Rosenberg RD. Molecular enhancement of porcine cardiac chronotropy. *Heart*. 2001;86:559–562.
32. Miake J, Marban E, Nuss HB. Functional role of inward rectifier current in heart probed by Kir2.1 overexpression and dominant-negative suppression. *J Clin Invest*. 2003;111:1529–1536.
33. Plotnikov AN, Sosunov EA, Qu J, Shlapakova IN, Anyukhovsky EP, Liu L, Janse MJ, Brink PR, Cohen IS, Robinson RB, Danilo P Jr, Rosen MR. Biological pacemaker implanted in canine left bundle branch provides ventricular escape rhythms that have physiologically acceptable rates. *Circulation*. 2004;109:506–512.
34. Qu J, Plotnikov AN, Danilo P Jr, Shlapakova I, Cohen IS, Robinson RB, Rosen MR. Expression and function of a biological pacemaker in canine heart. *Circulation*. 2003;107:1106–1109.
35. Potapova I, Plotnikov A, Lu Z, Danilo P Jr, Valiunas V, Qu J, Doronin S, Zuckerman J, Shlapakova IN, Gao J, Pan Z, Herron AJ, Robinson RB, Brink PR, Rosen MR, Cohen IS. Human mesenchymal stem cells as a gene delivery system to create cardiac pacemakers. *Circ Res*. 2004;94:952–959.
36. Kehat I, Khimovich L, Caspi O, Gepstein A, Shofti R, Arbel G, Huber I, Satin J, Itskovitz-Eldor J, Gepstein L. Electromechanical integration of cardiomyocytes derived from human embryonic stem cells. *Nat Biotechnol*. 2004;22:1282–1289.